

# Noise adaptive wavelet thresholding for speckle noise removal in optical coherence tomography

FARZANA ZAKI,<sup>1</sup> YAHUI WANG,<sup>1</sup> HAO SU,<sup>2</sup> XIN YUAN,<sup>3</sup> AND XUAN LIU<sup>1,\*</sup>

<sup>1</sup>Department of Electrical and Computer Engineering, New Jersey Institute of Technology, Newark, NJ 079102, USA

<sup>2</sup>School of Engineering and Applied Sciences, Harvard University, Cambridge, MA 02138, USA

<sup>3</sup>Bell Labs, Nokia, 600 Mountain Avenue, Murray Hill, NJ 07974, USA

\*xliu@njit.edu

**Abstract:** Optical coherence tomography (OCT) is based on coherence detection of interferometric signals and hence inevitably suffers from speckle noise. To remove speckle noise in OCT images, wavelet domain thresholding has demonstrated significant advantages in suppressing noise magnitude while preserving image sharpness. However, speckle noise in OCT images has different characteristics in different spatial scales, which has not been considered in previous applications of wavelet domain thresholding. In this study, we demonstrate a noise adaptive wavelet thresholding (NAWT) algorithm that exploits the difference of noise characteristics in different wavelet sub-bands. The algorithm is simple, fast, effective and is closely related to the physical origin of speckle noise in OCT image. Our results demonstrate that NAWT outperforms conventional wavelet thresholding.

© 2017 Optical Society of America

**OCIS codes:** (110.4500) Optical coherence tomography, (030.6140) Speckle, (100.3020) Image reconstruction-restoration, (110.4280) Noise in imaging systems.

## References and links

1. D. Huang, E. A. Swanson, C. P. Lin, J. S. Schuman, W. G. Stinson, W. Chang, M. R. Hee, T. Flotte, K. Gregory, C. A. Puliafito, and et, "Optical coherence tomography," *Science* **254**(5035), 1178–1181 (1991).
2. A. F. Fercher, W. Drexler, C. K. Hitzenberger, and T. Lasser, "Optical coherence tomography-principles and applications," *Rep. Prog. Phys.* **66**(2), 239–303 (2003).
3. A. M. Zysk, F. T. Nguyen, A. L. Oldenburg, D. L. Marks, and S. A. Boppart, "Optical coherence tomography: a review of clinical development from bench to bedside," *BIOMEDO* **12**, 051403 (2007).
4. J. W. Goodman, *Statistical Optics* (John Wiley & Sons, 2015).
5. J. W. Goodman, "Some fundamental properties of speckle," *J. Opt. Soc. Am.* **66**(11), 1145–1150 (1976).
6. X. Liu, J. C. Ramella-Roman, Y. Huang, Y. Guo, and J. U. Kang, "Robust spectral-domain optical coherence tomography speckle model and its cross-correlation coefficient analysis," *J. Opt. Soc. Am. A* **30**(1), 51–59 (2013).
7. J. M. Schmitt, S. H. Xiang, and K. M. Yung, "Speckle in Optical Coherence Tomography," *J. Biomed. Opt.* **4**(1), 95–105 (1999).
8. M. Bashkansky and J. Reintjes, "Statistics and reduction of speckle in optical coherence tomography," *Opt. Lett.* **25**(8), 545–547 (2000).
9. N. Iftimia, B. E. Bouma, and G. J. Tearney, "Speckle reduction in optical coherence tomography by "path length encoded" angular compounding," *J. Biomed. Opt.* **8**(2), 260–263 (2003).
10. M. Pircher, E. Götzinger, R. Leitgeb, A. F. Fercher, and C. K. Hitzenberger, "Speckle reduction in optical coherence tomography by frequency compounding," *J. Biomed. Opt.* **8**(3), 565–569 (2003).
11. D. P. Popescu, M. D. Hewko, and M. G. Sowa, "Speckle noise attenuation in optical coherence tomography by compounding images acquired at different positions of the sample," *Opt. Commun.* **269**(1), 247–251 (2007).
12. A. Ozcan, A. Bilencu, A. E. Desjardins, B. E. Bouma, and G. J. Tearney, "Speckle reduction in optical coherence tomography images using digital filtering," *J. Opt. Soc. Am. A* **24**(7), 1901–1910 (2007).
13. J. Rogowska and M. E. Brezinski, "Evaluation of the adaptive speckle suppression filter for coronary optical coherence tomography imaging," *IEEE Trans. Med. Imaging* **19**(12), 1261–1266 (2000).
14. R. C. Gonzalez and R. E. Woods, "Image processing," in *Digital Image Processing* (Pearson, 2007).
15. S. Sudha, G. Suresh, and R. Sukanesh, "Speckle noise reduction in ultrasound images by wavelet thresholding based on weighted variance," *IJACTE* **1**, 7–12 (2009).

16. H. Guo, J. E. Odegard, M. Lang, R. A. Gopinath, I. W. Selesnick, and C. S. Burrus, "Wavelet based speckle reduction with application to SAR based ATD/R," in *Image Processing, 1994. Proceedings. ICIP-94., IEEE International Conference, (IEEE, 1994)*, 75–79.
17. D. C. Adler, T. H. Ko, and J. G. Fujimoto, "Speckle reduction in optical coherence tomography images by use of a spatially adaptive wavelet filter," *Opt. Lett.* **29**(24), 2878–2880 (2004).
18. S. G. Chang, B. Yu, and M. Vetterli, "Adaptive wavelet thresholding for image denoising and compression," *IEEE Trans. Image Process.* **9**(9), 1532–1546 (2000).
19. S. G. Chang, B. Yu, and M. Vetterli, "Spatially adaptive wavelet thresholding with context modeling for image denoising," *IEEE Trans. Image Process.* **9**(9), 1522–1531 (2000).
20. X. Liu, Y. Huang, and J. U. Kang, "Distortion-free freehand-scanning OCT implemented with real-time scanning speed variance correction," *Opt. Express* **20**(15), 16567–16583 (2012).
21. X. Liu, M. Kirby, and F. Zhao, "Motion analysis and removal in intensity variation based OCT angiography," *Biomed. Opt. Express* **5**(11), 3833–3847 (2014).
22. Y. Qiu, Y. Wang, K. D. Belfield, and X. Liu, "Ultrathin lensed fiber-optic probe for optical coherence tomography," *Biomed. Opt. Express* **7**(6), 2154–2162 (2016).
23. F. Sattar, L. Floreby, G. Salomonsson, and B. Lovstrom, "Image enhancement based on a nonlinear multiscale method," *IEEE Trans. Image Process.* **6**(6), 888–895 (1997).
24. P. Li, L. Zhou, Y. Ni, Z. Ding, and P. Li, "Angular compounding by full-channel B-scan modulation encoding for optical coherence tomography speckle reduction," *J. Biomed. Opt.* **21**(8), 086014 (2016).

## 1. Introduction

Optical coherence tomography (OCT) is a high-speed, high resolution, three-dimensional imaging technique based on low coherence light interferometry [1]. OCT has various applications in biomedicine, such as assisting clinical diagnosis in ophthalmology or guiding interventional procedures in cardiology [2, 3]. OCT, like other coherence imaging modalities, inevitably suffers from random noises particularly the multiplicative speckle noise [4–6]. Speckle noise in OCT image randomly modulates the magnitude of OCT signal and obscures subtle image features, resulting in compromised effectiveness in its clinical applications [7, 8]. Various hardware and software based approaches have been developed to remove speckle noise. Hardware compounding for speckle noise reduction, such as spatial compounding and spectral compounding, may achieve higher signal to noise ratio (SNR) of OCT images, while compromise system cost, spatial resolution, and imaging speed [9–11]. On the other hand, post-processing algorithms have also been developed to reduce speckle noise in OCT images [12, 13]. Since speckle noise is inherently multiplicative rather than additive, conventional linear filtering in spatial or frequency domain is suboptimal, producing significant blurring and reducing image contrast [14]. Wavelet thresholding methods that are nonlinear have been used for speckle noise removal in various imaging modalities including ultrasound imaging, synthetic aperture imaging and OCT [15–17]. Wavelet thresholding algorithms have demonstrated excellent capability in reducing speckle noise and preserving image sharpness [18, 19]. The underlying principle of wavelet thresholding is that the magnitude of wavelet coefficients can be used as an oracle to determine if a coefficient is noise or signal. A wavelet coefficient with larger amplitude is more likely to carry important information while a wavelet coefficient with smaller amplitude is more likely to be noise.

In previous implementation of wavelet domain thresholding for OCT image noise reduction, an adaptive threshold was determined for each wavelet sub-band using an estimated signal variance for the specific sub-band and the same magnitude of noise variance for all sub-bands, assuming the noise level is the same in different wavelet sub-bands. However, we have demonstrated in our previous study that the de-correlation of OCT signals with fully developed speckle could be modeled as a Gaussian function, suggesting a Gaussian power spectral density for speckle noise [20]. Therefore, the speckle pattern in OCT image has different magnitudes at different spatial scales or in different wavelet sub-bands. On the other hand, the characteristics of speckle noise are largely determined by the imaging system rather than the sample. Therefore, it is possible to extract the characteristics of speckle noise in a structureless OCT image obtained from a homogeneous scattering sample and

subsequently use these characteristics to remove speckle noise in OCT images obtained from other samples.

To achieve better performance in speckle noise removal, here we study a novel algorithm for OCT speckle noise removal. In our noise adaptive wavelet thresholding (NAWT) strategy, we first acquired and analyzed an OCT image of a homogeneous scattering sample, quantified the noise variance ( $\sigma_w^2$ ) in individual wavelet sub-band, and used  $\sigma_w^2$  to determine the optimal threshold for individual sub-band. The algorithm is simple, fast, effective and is closely related to the physical origin of speckle noise in OCT image. Our results clearly demonstrated the advantage of the NAWT algorithm compared to conventional wavelet domain thresholding and linear filtering.

## 2. Principle

In conventional wavelet thresholding method, spatial domain image is first transformed to wavelet domain (Fig. 1). Afterwards, a data driven threshold ( $T$ ) is determined using Eq. (1) for each sub-band of detail coefficients ( $H_1, V_1, D_1, H_2, V_2, D_2, H_3, V_3, D_3, \dots$ ), where  $H_k$  indicates detail coefficients in horizontal direction at  $k^{\text{th}}$  wavelet decomposition level;  $V_k$  indicates detail coefficients in vertical direction at  $k^{\text{th}}$  wavelet decomposition level, and  $D_k$  indicates detail coefficients in diagonal direction at  $k^{\text{th}}$  wavelet decomposition level. In Eq. (1),  $\sigma^2$  indicates the noise variance and  $\sigma_x$  indicates the standard derivation of noise-free signal. Using the data-driven thresholding, Eq. (2) a.k.a. soft thresholding is applied to each wavelet coefficient  $S$ . Spatial domain image with reduced speckle noise is then reconstructed through inverse wavelet transform. Noise variance ( $\sigma^2$ ) used in Eq. (1) is estimated using the detail subband  $H_1$  by the robust median estimator as shown in Eq. (3). The standard derivation of the noise free signal in ( $\sigma_x$ ) each wavelet sub-band is estimated using Eq. (4), where  $\sigma_s^2$  is the variance of the measured wavelet coefficients. The close form threshold calculated in Eq. (1) leads to optimal noise reduction, given the wavelet coefficients of OCT image following a generalized Gaussian distribution (GGD). Equations (1)–(4) summarize the procedure of conventional adaptive wavelet thresholding for image denoising, as described by S. G. Chang *et al* in [18]. However, the assumption that the noise variance ( $\sigma^2$ ) is the same across all the sub-bands in wavelet domain is not valid for OCT signal, because the speckle in OCT signal has different characteristics in different spatial scales. Therefore, we propose a noise adaptive wavelet thresholding (NAWT) algorithm that takes different characteristics of speckle noise at different spatial scale to achieve more effective noise reduction.

$$T(\sigma_x) = \frac{\sigma^2}{\sigma_x} \quad (1)$$

$$S_T = \begin{cases} 0; & |S| \leq T \\ \text{sgn}(S)[|S| - T]; & |S| > T \end{cases} \quad (2)$$

$$\sigma = \frac{\text{Median}(|S_{ij}|)}{0.6745}, \quad S_{ij} \in \text{subband } H_1 \quad (3)$$

$$\sigma_x = \sqrt{\max(\sigma_s^2 - \sigma^2, 0)} \quad (4)$$

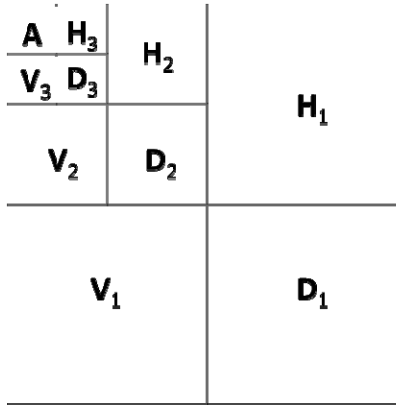


Fig. 1. 2D wavelet decomposition of an image.

The major difference between our NAWT algorithm and conventional wavelet domain thresholding is that NAWT uses different noise variance to calculate the threshold for each sub-band. Specifically, we use Eq. (5) to estimate the threshold, where  $\sigma_w^2$  indicate the noise variance for the sub-band  $W$  ( $W$  will be all different sub-bands: H1, V1, D1, H2, V2, D2, H3, V3, D3, ...).  $\sigma_w^2$  for each sub-band is estimated using an image obtained from a structureless sample with homogeneous optical properties. The image is modulated by fully developed speckle. Wavelet domain speckle statistics extracted from the structureless sample can be applied to other images, as the speckle in OCT image is dependent primarily on the characteristics of the imaging system rather than the sample. In other words, our NAWT algorithm applies the noise variance at different sub-band of wavelet coefficients as a prior for subsequent noise reduction.

$$T_N(\sigma_x) = \frac{\sigma_w^2}{\sigma_x} \quad (5)$$

The reference image obtained from a uniform scattering sample allows the speckle noises characteristics to be characterized, because the magnitude variation in such a reference image can be attributed to random noise. On the other hand, it is impossible to assess speckle noise characteristics using an OCT image obtained from a spatially heterogeneous sample. In such an image, the magnitude of OCT image varies not only due to random noise, but also due to deterministic structural features of the sample.

The flow-chart for the NAWT algorithm is shown in Fig. 2. Briefly, we calculate  $\sigma_w^2$  for each subband (H1, V1, D1, H2, V2, D2, H3, V3, D3, ...) from the structureless reference image ( $\mathbf{R}_{xy}$ ) that is obtained from the homogeneous scattering sample. Afterwards, we use the image to be denoised ( $\mathbf{S}_{xy}$ ) to estimate the signal variance (Eq. (4)). The threshold for each sub-band is thus estimated using Eq. (5). Notably,  $\mathbf{R}_{xy}$  and  $\mathbf{S}_{xy}$  are normalized by their mean signal intensities respectively. Every wavelet coefficient ( $S$ ) in a detail sub-band is then thresholded using Eq. (2). Spatial domain image is then reconstructed via inverse wavelet transform. The algorithm is implemented in Matlab 2016 on a personal computer (intel i72.8 GHz CPU, 8GB memory). The time to process a 512x2014 image is approximately 0.2s.

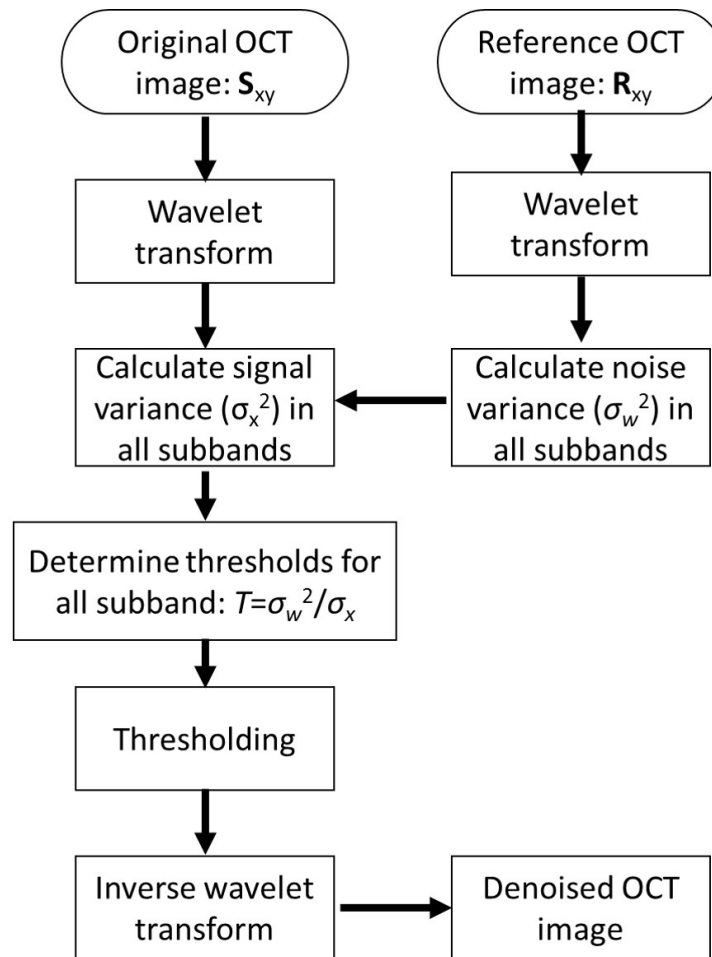


Fig. 2. Signal processing flow chart for the optimized adaptive wavelet thresholding algorithm.

### 3. OCT imaging system

We used a spectral domain OCT (SD OCT) system for imaging experiments. Details about this system can be found in our previous publications [21, 22]. The SD-OCT system has a superluminescent diode (SLD1325 Thorlabs, 1.3 $\mu$ m central wavelength and 100nm bandwidth, power smaller than 10mW at the sample) as the broadband light source. The output of the SLD illuminates the reference and sample arm of a fiber-optic Michelson interferometer through a fiber-optic coupler. A lens is used in the sample arm to focus the probing beam and collect photons backscattered from the sample. Light returned from the sample and the reference mirror interferes and is detected by a CMOS InGaAs camera (SUI1024LDH2, Goodrich). A frame grabber (PCIe-1433, National Instrument) streams the signal from the camera to the host computer (Dell Precision T7600) where the OCT signal is processed in real-time using GPU.

### 4. Results

We first assessed the characteristics of speckle noise of OCT image in wavelet domain. In order to do this, we imaged a homogeneous scattering phantom. The scattering phantom was made by curing Polydimethylsiloxane (PDMS)/titanium dioxide (TiO<sub>2</sub>) mixture. We acquired four structureless images (one of the images is shown in Fig. 3) from the same scattering

phantom using difference elevation planes (Bscan 1, Bscan 2, Bscan 3 and Bscan 4) with  $31.4\mu\text{m}$  interval. To analyze OCT speckle statistics, we normalized these images (linear scale) using their respective mean values, and calculated the probability density of signal magnitudes (for signals from  $0.8\text{mm}$  to  $1.15\text{mm}$  in depth), as shown in Fig. 4 (solid curves). In Fig. 4, we also plot the probability density function (PDF) of Rayleigh distribution with a mean of 1 ( $P(s) = \frac{s}{\sigma^2} \exp\left(-\frac{s^2}{2\sigma^2}\right)$  where  $\sigma = \sqrt{\frac{2}{\pi}}$ ), as the dashed curve. Clearly, images obtained from different elevation planes followed the same Rayleigh distribution, although they had different sub-resolution characteristics. This is consistent with our previous discussion that the speckle statistics of OCT image is determined largely by the imaging system rather than the sample properties, suggesting speckle statistics characterized using a reference image can be applied as a prior for subsequent noise reduction.

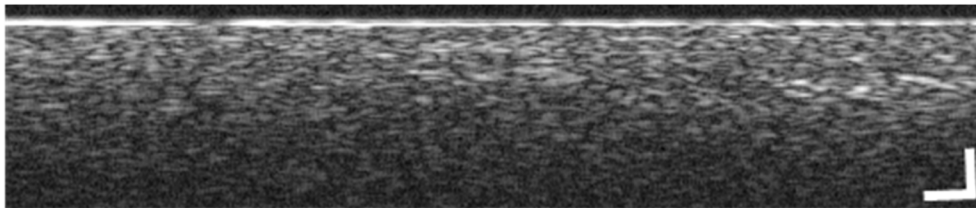


Fig. 3. OCT Bscan of the scattering phantom. Scale bars indicate  $200\ \mu\text{m}$ .

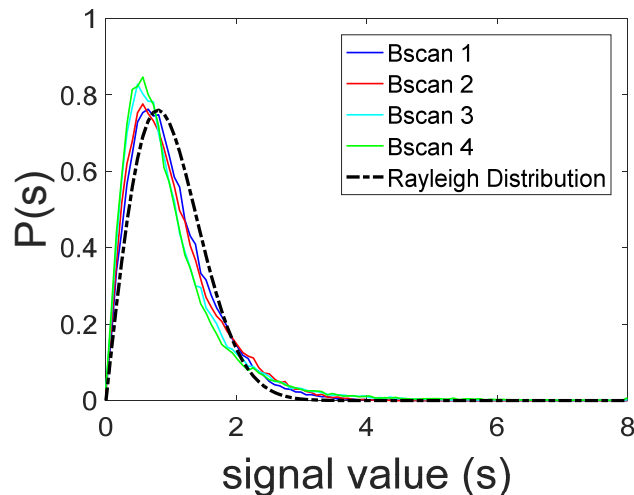


Fig. 4. Probability distribution of OCT signal magnitude (solid curves), in comparison with the PDF of Rayleigh distribution (dashed).

To demonstrate that the magnitude of speckle noise varies significantly between different wavelet sub-bands, we transformed one of the Bscan images (linear scale, normalized to its maximum value) obtained from the scattering phantom through into wavelet domain. A four-level wavelet transformation was performed using a sym4 wavelet base. For images obtained from a homogeneous scattering sample (Fig. 3), the variation of signal is simply due to noise. We calculated the variance of wavelet coefficients in horizontal (H), vertical (V) and diagonal (D) directions in four different decomposition levels (Fig. 5). Clearly, the magnitudes of noise quantified by wavelet coefficient variance are significantly different in different sub-bands. On the other hand, threshold for wavelet domain de-noising has been conventionally determined using Eq. (1), based on the assumption that noise variance ( $\sigma^2$ ) remains constant

across different wavelet sub-bands. However, Fig. 5 shows large difference for noise magnitude in different sub-bands, and soft-thresholding based on Eq. (1) is hence sub-optimal.

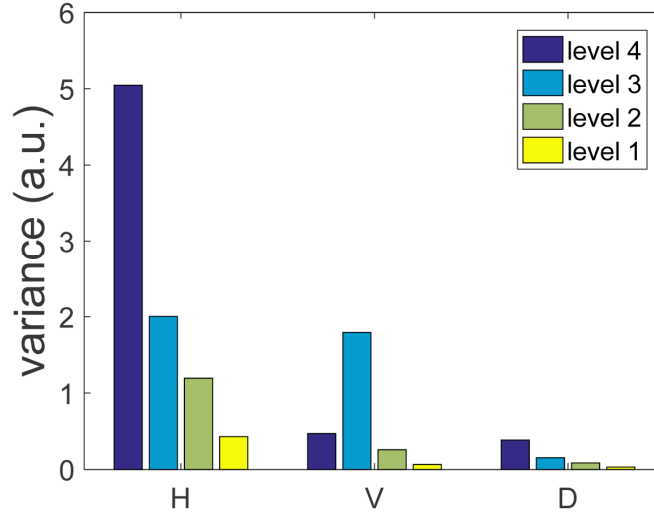


Fig. 5. Variance of wavelet coefficients for Bscan image obtained from the homogeneous scattering sample, in H, V, and D directions at four decomposition levels. Clearly, the magnitudes of noise quantified by wavelet coefficient variance are different in different sub-bands.

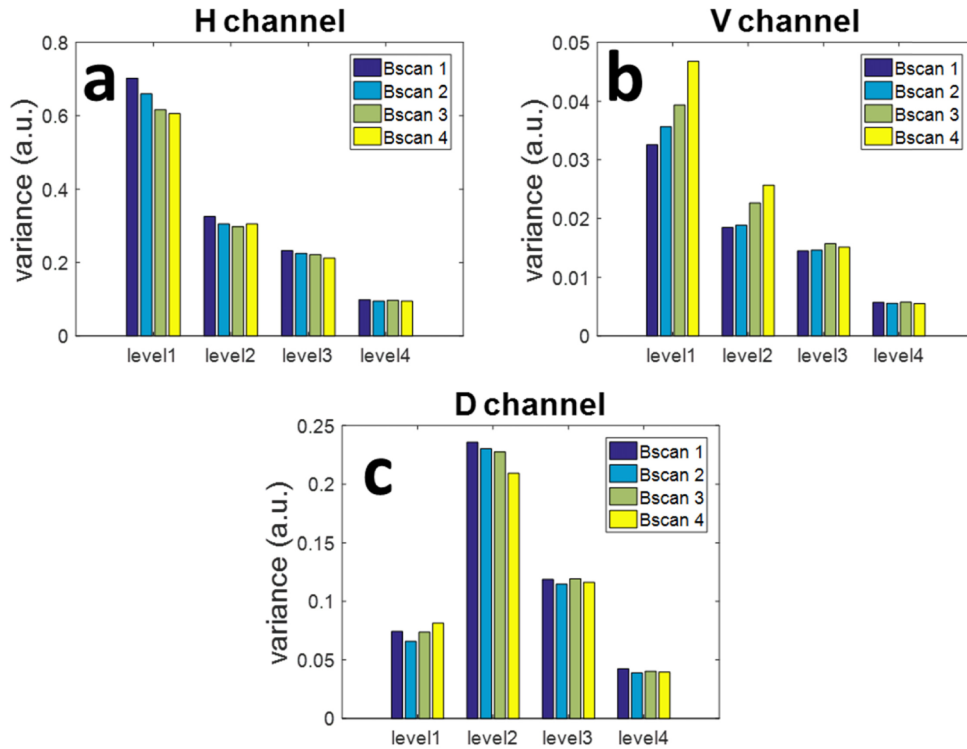


Fig. 6. Variance of wavelet coefficients for Bscan image obtained from the homogeneous scattering sample in four different elevation planes (Bscan 1, Bscan 2, Bscan 3, and Bscan 4), in H, V, and D directions at four decomposition levels.

To further validate that speckle statistics characterized using a reference image can be applied as a prior for subsequent noise reduction, we compared the inter-image difference for noise variance. Images (linear, normalized) obtained from the homogeneous scattering phantom is used to generate results shown in Fig. 6. For the same wavelet sub-band (H, V or D direction, level 1, 2, 3, or 4), the difference in noise variance between different images (Bscan1, Bscan 2, Bscan 3, and Bscan 4) is much smaller, compared to the difference between different wavelet sub-bands for the same image.

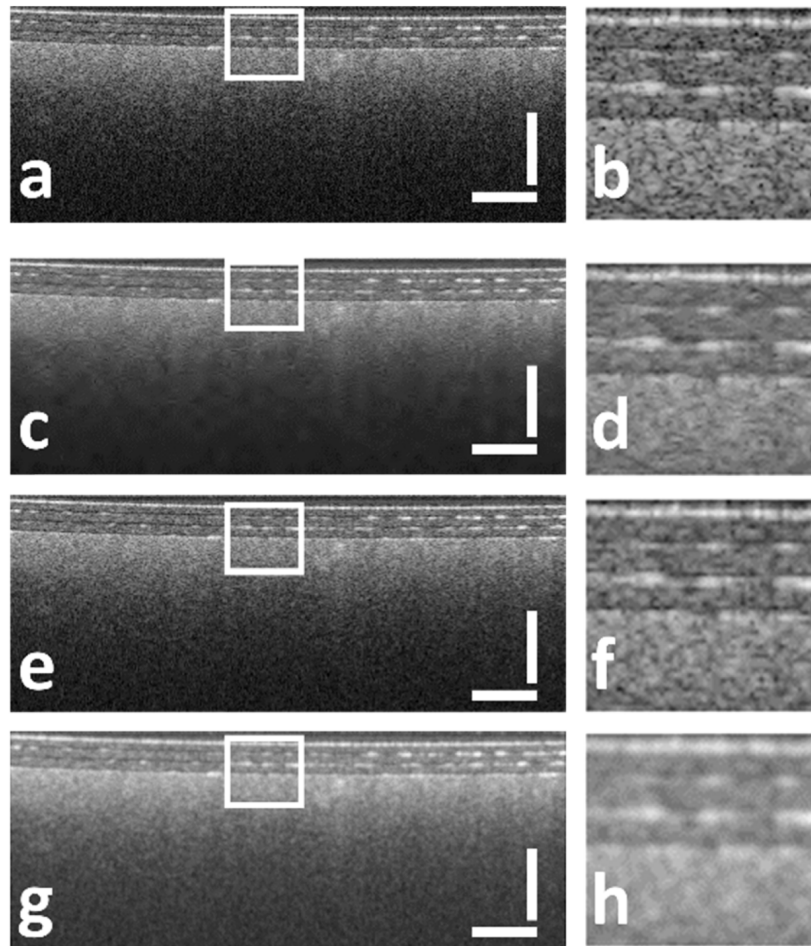


Fig. 7. (a) raw OCT image of Sample 1 (without any post processing); (b) enlarger region of interest (ROI) enclosed by the rectangle in Fig. 7(a); (c) OCT image of Sample 1 processed by our NAWT algorithm; (d) enlarger ROI enclosed by the rectangle in Fig. 7(c); (e) OCT image of Sample 1 processed by conventional wavelet domain thresholding; (f) enlarger ROI enclosed by the rectangle in Fig. 7(e); (g) OCT image of Sample 1 processed by Gaussian filtering; (h) enlarger ROI enclosed by the rectangle in Fig. 7(g). Scale bars in Fig. 7(a) indicate 500  $\mu\text{m}$ .

To demonstrate the efficacy of our algorithm, we applied our NAWT algorithm on a sample (Sample 1) made by attaching three layers of tapes on top of the homogeneous scattering phantom. The sample had well developed speckle pattern and had easily discernable layer structure, and hence was ideal for the validation of our NAWT algorithm. OCT image without any post-processing is shown in Fig. 7(a). The area within the rectangle is enlarged in Fig. 7(b) to provide better visualization of image details. The grainy appearance of the image is due to speckle noise. To perform speckle noise reduction using our NAWT

algorithm, we used the noise variance obtained from the homogeneous sample shown in Fig. 3 to generate the noise data driven adaptive threshold using Eq. (5). OCT image was then denoised following the procedures shown in Fig. 2. The resultant image is shown in Fig. 7(c) and a region of interest is enlarged in Fig. 7(d). Clearly, Fig. 7(c) and 7(d) show reduced noise compared to Fig. 7(a) and 7(b). In addition, the boundaries remain clear in Fig. 7(c) and 7(d). To demonstrate the advantage of our NAWT algorithm, we also processed Fig. 7(a) using conventional wavelet domain thresholding algorithm, and show the result in Fig. 7(e) and 7(f). The image texture remains grainy after denoise, compared to the result obtained from NAWT processing. We also performed spatial domain linear filtering using a Gaussian kernel (25 pixels by 25 pixels with a standard deviation  $\sigma$  equal to 1.5 pixels:  $h(i,j) = \exp[-(i^2 + j^2)/2\sigma^2]$ ) and show the result in Fig. 7(g) and 7(h). Gaussian filter effectively removed speckle noise, but reduced image contrast and blurred small features in the image.

To better illustrate the effectiveness of our NAWT algorithm in speckle noise reduction, we selected Ascans at the same lateral location from OCT images processed with different algorithms, and show the data in Fig. 8. OCT data without any enhancement (red curve) show random fluctuation due to the existence of speckle noise. The green curve that was obtained by conventional wavelet thresholding shows reduced noise variation. The noise is further reduced by processing the image with NAWT (blue curve), suggesting its superior performance for speckle noise suppression compared to conventional wavelet domain thresholding. The Ascans processed by the Gaussian filter (black curve) shows broadened signal peaks. This is consistent with the visual observation on Fig. 7(e) and 7(g) where Gaussian filtering blurs small structural features and reduces the contrast of the image. Particularly, Gaussian filtering reduces random fluctuation of the signal but results in artificially elevated the noise floor (depth >0.3mm), because Gaussian filter is linear and is not optimized for multiplicative speckle noise.

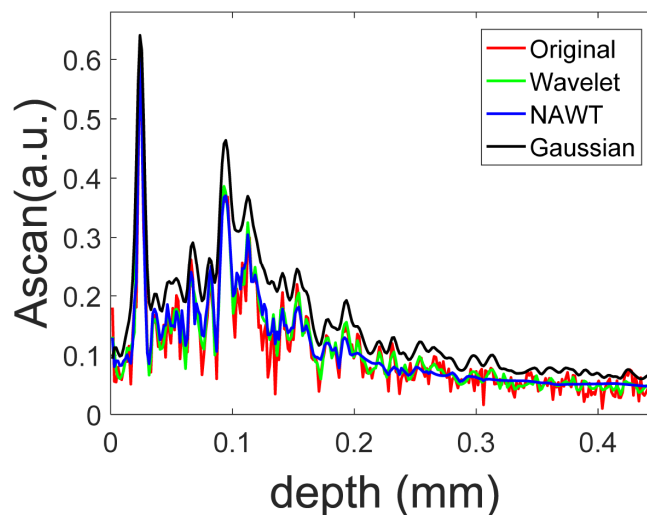


Fig. 8. Ascans at the same lateral location from OCT images processed with different algorithms.

We also applied our NAWT algorithm to OCT images obtained from an IR viewing card (Sample 2). OCT images without and with NAWT processing are shown in Fig. 9(a) and 9(b), respectively. Clearly, NAWT algorithm significantly reduced the grainy appearance of the image due to speckle noise. In addition, high spatial frequency features in the image such as the upper and lower boundaries of the plastic film are not blurred. We also acquired OCT image from human fingertip (Sample 3) (Fig. 9(c), original). The image processed by NAWT

is shown in Fig. 9(d) where the visibility of the epidermis-dermis junction is significantly enhanced.

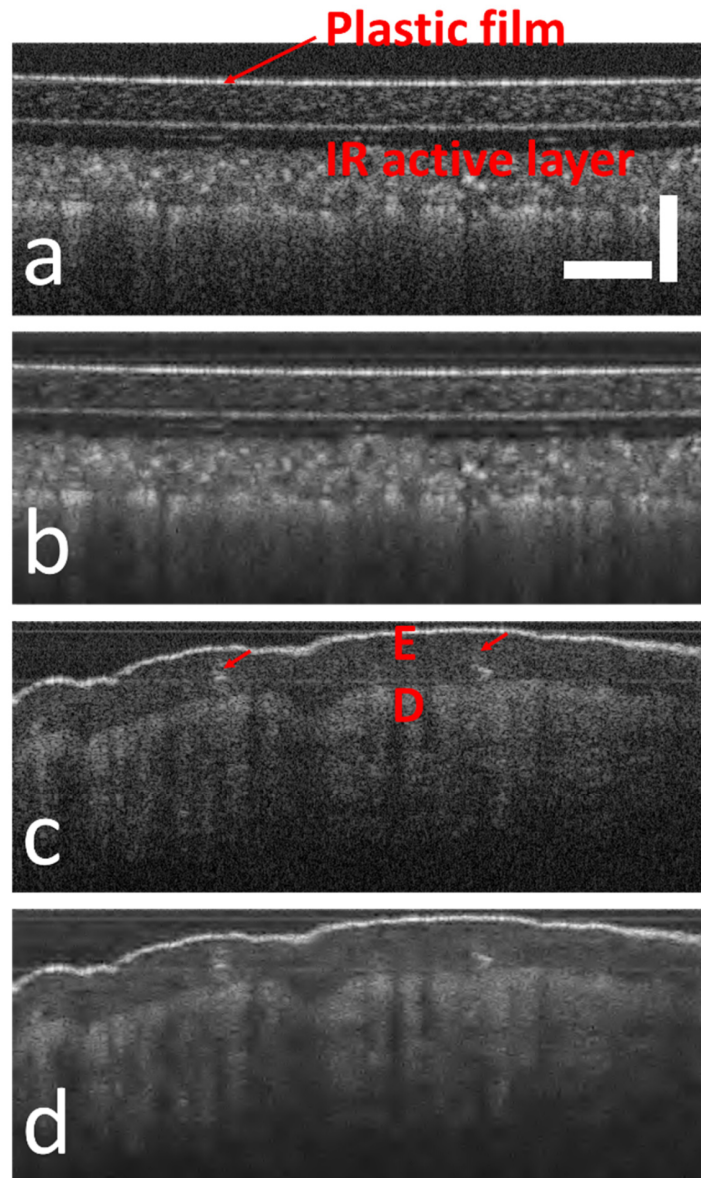


Fig. 9. (a) Original IR card image (Sample 2), (b) IR card image processed using NAWT; (c) fingertip image (Sample 3), (d) fingertip image processed using NAWT. Scale bars indicates 500  $\mu\text{m}$ . E: epidermis; D dermis; arrows in Fig. 9(c) indicate sweat duct.

To quantitatively assess the effectiveness of different speckle removal algorithms, we calculated the SNR of the OCT images (Eq. (6) where  $\mu_I$  indicates the mean of the OCT image and  $\sigma_I^2$  indicates noise variance of the OCT image) [17,24]. Notably, the noise variance for SNR calculation was obtained using OCT data within the depth range from 1mm-1.5mm. In addition, we used the parameter  $\beta$  (Eq. (7)) to assess the capability of a noise removal algorithm to preserve the structural feature of an image [23]. In Eq. (7),  $I_D$  indicates the denoised image;  $I_0$  indicates the original image;  $\mu_D$  indicates the mean signal value of the

denoised image;  $\mu_0$  indicates the mean signal value of the original image;  $\Gamma(I_1, I_2) = \sum_{i,j} [I_1(i, j)I_2(i, j)]$  where  $i$  and  $j$  indicate indices of pixel in 2D images. The parameter  $\beta$  essentially is a correlation coefficient that quantifies how well the denoised image preserves morphological features of the original image. The performance of speckle reduction algorithms (WT: conventional wavelet domain thresholding; NAWT: noise adaptive wavelet thresholding; GF: Gaussian filtering) is evaluated using OCT images obtained from Sample 1 (Fig. 7), Sample 2 (Fig. 9(a) and 9(b)), and Sample 3 (Fig. 9(c) and 9(d)). As shown in Table 1, our NAWT algorithm provides the most significant SNR improvement (3-8 dB) compared to other methods. On the other hand, NAWT has comparable effectiveness in preserving image features ( $\beta$  value) as compared with conventional wavelet domain thresholding, while outperforms Gaussian filtering. In Table 1, values corresponding to the best imaging performance are highlighted in bold.

$$SNR = 10 \log_{10} \left( \frac{\mu_I^2}{\sigma_I^2} \right) \tag{6}$$

$$\beta = \frac{\Gamma(I_D - \mu_{I_D}, I_0 - \mu_{I_0})}{\sqrt{\Gamma(I_D - \mu_{I_D}, I_D - \mu_{I_D}) \cdot \Gamma(I_0 - \mu_{I_0}, I_0 - \mu_{I_0})}} \tag{7}$$

Table 1. Performance of different noise reduction algorithms.

Parameters	Methods	Sample 1	Sample 2	Sample 3
SNR (dB)	Raw	17.13	11.42	13.56
	WT	23.17	13.24	17.99
	NAWT	<b>29.04</b>	<b>14.56</b>	<b>20.59</b>
	GF	25.04	14.07	18.99
	WT	0.96	<b>0.96</b>	<b>0.94</b>
$\beta$	NAWT	<b>0.97</b>	0.94	0.93
	GF	0.92	0.92	0.90

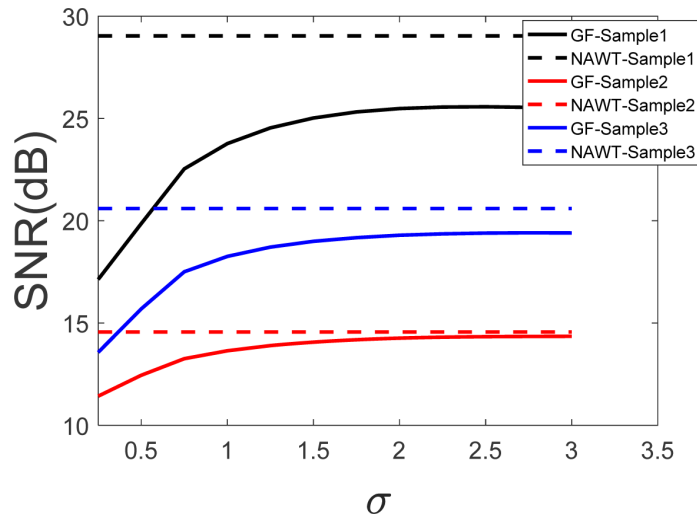


Fig. 10. SNR performance of Gaussian filtering and NAWT.

## 5. Conclusion and discussion

We have proposed and validated a novel algorithm to remove the speckle noise in OCT images. Our noise adaptive wavelet thresholding (NAWT) algorithm utilized the characteristics of speckle noise in wavelet domain to adaptively remove speckle noise while preserving structure features in OCT image. Our results demonstrated that NAWT led to improved visual appearance of OCT image. Moreover, we quantitatively demonstrated the superior performance of NAWT in noise removal by SNR and in preserving structural features by the quantity  $\beta$ , compared to conventional wavelet domain thresholding and Gaussian filtering.

We believe the application of the NAWT algorithm is not limited to OCT image. The effectiveness our algorithm derives from the fact that the speckle statistics is largely determined by the imaging system rather than the sample characteristics. This is true for most imaging/sensing technologies based on coherence detection of signal. Therefore, we expect the NAWT to be a generic algorithm for speckle noise removal in various imaging/sensing technologies, such as ultrasound imaging, synthetic aperture imaging, Lidar, etc. As long as the assumption of fully developed speckle is approximately satisfied, our algorithm can significantly improve the image quality through speckle noise suppression. Notably, as shown in Fig. 6, there is difference in noise variance between images obtained from different elevation planes of the same homogeneous sample, because of the stochastic nature of speckle noise. The difference in noise characteristics is even larger for different heterogeneous samples. However, for OCT images obtained from turbid media, such as most biological tissues, the expected value of OCT signal (magnitude) varies significantly only when the refractive index changes abruptly. Therefore, our NAWT method can effectively remove speckle noise for most pixels in OCT images obtained from turbid media.

The NAWT algorithm does not require massive computational power, and it takes approximately 0.2s to process a 512x1024 image using CPU in Matlab environment. The main steps of NAWT comprise wavelet decomposition, soft thresholding, and wavelet reconstruction. All these steps can be parallelized using graphic processing units (GPU). Therefore, the NAWT algorithm can be implemented in GPU for real-time speckle noise removal. The time complexity for our NAWT is the same as conventional wavelet thresholding. To perform NAWT, we estimate the noise variance in different wavelet sub-bands in advance from a structureless reference image. A threshold is calculated accordingly for each sub-band to reduce speckle noise. Therefore, the major difference between NAWT and conventional wavelet thresholding is the approach for the calculation of noise variance, while the computation procedures for speckle noise removal remain the same.